

This document is the unedited Author's version of a Submitted Work that was subsequently accepted for publication in the Journal of the American Chemical Society, copyright © American Chemical Society after peer review. To access the final edited and published work see <http://pubs.acs.org/articlesonrequest/AOR-5EmE5s7CqW6U5nPDwUkM>.

Chasing the Evasive Fe=O Stretch and the Spin State of the Iron(IV)-Oxo Complexes by Photodissociation Spectroscopy

Erik Andris,[‡] Rafael Navrátil,[‡] Juraj Jašík,[‡] Terencio Thibault,[‡] Martin Srnec,^{‡*} Miquel Costas,^{†*} and Jana Roithová^{‡*}

[‡] Department of Organic Chemistry, Faculty of Science, Charles University, Hlavova 2030/8, 12843 Prague 2 (Czech Republic).

[†] Departament de Química and Institute of Computational Chemistry and Catalysis (IQCC), University of Girona, Campus Montilivi, Girona 17071 (Spain).

[‡] J. Heyrovsky Institute of Physical Chemistry of the CAS, v. v. i., Dolejškova 2155/3, 182 23 Prague 8 (Czech Republic)

ABSTRACT: We demonstrate the application of infrared photodissociation spectroscopy for determination of the Fe=O stretching frequencies of high-valent iron(IV)-oxo complexes $[(L)Fe(O)(X)]^{2+/+}$ ($L = TMC, N_4Py, PyTACN$, and $X = CH_3CN, CF_3SO_3, ClO_4, CF_3COO, NO_3, N_3$). We show that the values determined by resonance Raman spectroscopy in acetonitrile solutions are in average 9 cm^{-1} red-shifted with respect to unbiased gas-phase values. Furthermore, we show the assignment of the spin state of the complexes based on the vibrational modes of a coordinated anion and compare reactivities of various iron(IV)-oxo complexes generated as dications or monocations (bearing the anionic ligand). The coordinated anions can drastically affect the reactivity of the complex and should be taken into account when comparing reactivities of complexes bearing different ligands. Comparison of reactivities of $[(PyTACN)Fe(O)(X)]^+$ generated in different spin-states and bearing different anionic ligands X revealed that the nature of anion influences the reactivity more than the spin-state. The triflate and perchlorate ligands tend to stabilize the quintet state of $[(PyTACN)Fe(O)(X)]^+$, whereas trifluoroacetate and nitrate stabilize the triplet state of the complex.

INTRODUCTION

Non-heme high-valent iron-oxo chemistry is a rapidly evolving field with interdisciplinary connections between organic, inorganic and theoretical chemistry. The importance of non-heme iron-oxo compounds in many enzymatic reactions¹ has been appreciated mainly after the seminal works of Bollinger and Krebs.² Our understanding of these reactive species and their function has been to a great extent facilitated by the development of their synthetic models.^{3,4} Characterization of the active iron centers currently relies mainly on UV/VIS, Mössbauer, resonance Raman, EPR and X-Ray spectroscopic techniques.⁵ Usually, resonance Raman (rR) spectroscopy provides the most direct evidence for the Fe=O moiety.^{4a,6} The rR method takes advantage of resonance enhancement and thus relies on the presence of intense electronic absorption features.⁷ These are, however, not always present.^{8,9} In addition, they have limitations when dealing with complex mixtures. As a result, minor - though important - species may stay unnoticed. As numerous reported, mass spectrometry is an ideal tool for detection of reactive species present in low concentrations (dynamic range of a standard mass spectrometer is $\sim 10^4$ - 10^6).¹⁰⁻¹² The requirement of detailed structural information on the detected ions urged the development of

novel techniques that combine MS with other spectroscopic methods such as infrared (IR) spectroscopy.¹³

Our approach, helium tagging infrared photodissociation spectroscopy (IRPD), consists in trapping the ions of interest in a cryogenic ion trap ($\sim 3\text{ K}$) filled with helium. The ions are collisionally cooled and form weakly bound complexes with helium atoms. The complexes, irradiated by a tunable IR beam, detach helium if they absorb a photon. Hence, we obtain IR spectra as a dependence of the depletion of the helium complexes on the IR wavenumber.¹⁴

Herein we report a set of IRPD spectra of representative non-heme iron(IV)-oxo complexes with a special emphasis on the Fe=O stretching vibration. The interface of electrospray ionization (ESI) serves to transfer the complexes from their acetonitrile solution to the gas phase. Assignment of vibrational bands to the Fe=O stretching modes is based on the ^{18}O labeling, which has been done by the oxygen atom exchange with $H_2^{18}O$ (Chart 1).¹⁵

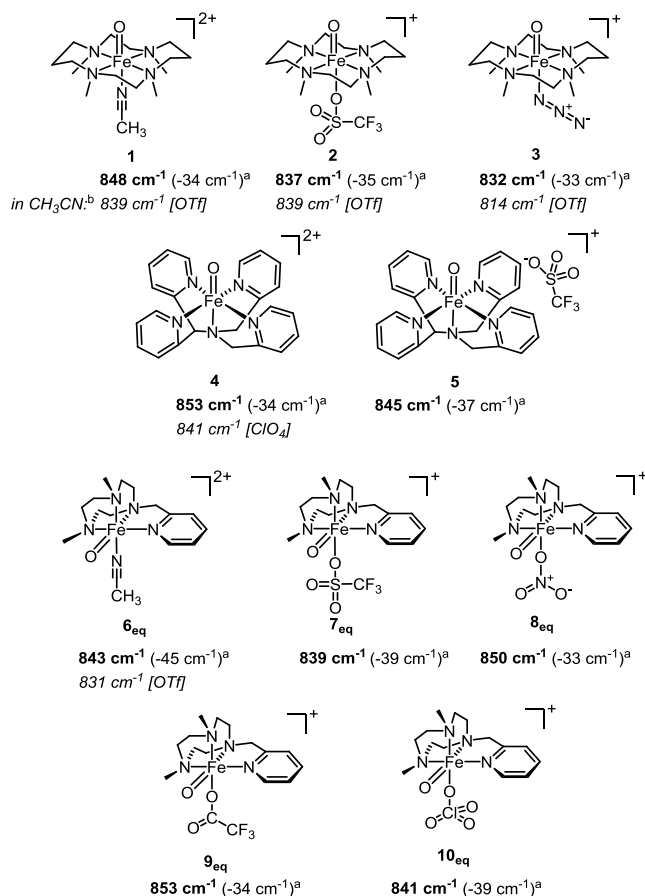


Chart 1. Investigated complexes and their Fe=O stretching frequencies.^a

^aSpectral shift upon ¹⁸O labeling.

^bFrequencies of the complexes measured in acetonitrile solution by rR spectroscopy taken from Ref. 6b are given in italics. Present counter ions are given in brackets.

EXPERIMENTAL AND COMPUTATIONAL DETAILS

Ion-molecule reactivity studies: Experiments were performed with a triple quadrupole mass spectrometer TSQ 7000.¹⁶ Complexes **1**, **2** and **4–7** (Chart 1) were prepared according to the corresponding literature procedures^{5,17} by oxidation of the corresponding iron(II) triflate precursors dissolved in acetonitrile (typically 0.1–1 mM) by either iodosobenzene (**1**, **2**, **4**, **5**) or peracetic acid (**6–7**). Complex **3** was generated from the solution containing **1** by addition of 1 eq. NaN₃. Complexes **8–10** were prepared by addition of 2, 0.3 and 2 equivalents of the corresponding acid to the solution containing **6**. The complexes were transferred to the gas phase by an ESI ion source at mild ionization conditions (low voltage differences during the transfer and temperature ~ 60 °C). Alternatively, complexes **7–10** were generated by the NO₂ elimination from their [(PyTACN)Fe(NO₃)(X)]⁺ precursors during the electrospray ionization. The NO₂ elimination requires harder ionization conditions (larger voltage differences between the transfer capillary and lenses).

Generated iron-oxo complexes were mass-selected by the first quadrupole and reacted with a neutral reactant at thermal conditions (nominally zero collision energy, Figure S1).¹⁶ Product ions were mass-analyzed by the second quadrupole. Reaction rates were extracted from the pressure dependence of the relative abundance of the products on the reactant gas pressure.¹⁸ Further details regarding generation of the ions and their reactivity are in the Supporting Information.

IRPD spectra: The IRPD spectra were acquired with the ISORI instrument.¹⁹ The ions were prepared in the same way as mentioned above, mass selected by the first quadrupole and transferred via an octopole to a cryo-cooled wire quadrupole ion trap operated at 3 K and 1 Hz. The ions were trapped with pulsed helium buffer gas (for the time sequence of the experiment see Figure S2 in the Supporting Information). About 1–10% of the trapped ions were transformed to the He tagged complexes. After a time delay, the ion cloud was irradiated by 8 photon pulses generated in an optical parametric oscillator/amplifier (OPO) operating at 10 Hz frequency. At 990 ms, the exit electrode of the trap was opened, the helium-tagged ions were mass-analyzed by the second quadrupole, and their number (*N*) was determined by the Daly-type detector operated in the ion-counting mode. In the following cycle, the light from the OPO was blocked by a mechanical shutter, giving the number of unirradiated ions (*N*₀). The IRPD spectra are constructed as the wavenumber dependence of (1 - *N*/*N*₀). Wavenumber calibration was done using the absorption of methane and water (Figure S3) and our accuracy is ± 3 cm⁻¹ (precision is ± 1 cm⁻¹). In the cases of **5**, **7**, and **8**, lambdameter WS-600 from HighFinesse GmbH was used for accurate determination of wavelength.

DFT calculations: Geometry optimizations and frequency calculations were performed using different density functional theory methods and triple-ζ basis sets as implemented in Gaussian 09.²⁰ The basis set was constructed as a combination of 6-311++G** for C, H, O, Fe, F and N atoms (pure for **6** and **8**) and pc-3^{21,22} for S and Cl atoms and also for the carbon atom in the CF₃ group (concerns **7** and **9**). The combined basis set is abbreviated as BS1. All optimized structures are minima on the potential energy surface confirmed by diagonalization of the mass-weighted Hessian matrix. The calculated IR spectra were scaled by factor 0.99.

CASSCF/CASPT2 calculations: The complete active space self-consistent field (CASSCF)²³ and complete active space second-order perturbation theory (CASPT2)²⁴ calculations were carried out using the MOLCAS 8.0 program.²⁵ For all of the atoms, the ANO-RCC basis set, contracted to [6s5p3d2f1g] for Fe, [4s3p2d] for the ligating O, N atoms, [3s2p] for other N, O, F and C atoms, [4s3p] for Cl and S atoms, and [2s] for H, was used. The second-order Douglas-Kroll-Hess (DKH2) one-electron spinless Hamiltonian was applied for all of the calculations in order to allow for spin-free relativistic effects.²⁶

The CASSCF energies were calculated for the B3LYP-optimized geometries with the 12-electrons-in-9-orbitals active space including 5×3*d*_{Fe}, 3×2*p*_{OxO} and 1σ chelate-based orbital. To improve the accuracy of the calculations, the CASPT2 energies were used on the diagonal of the two-component Hamiltonian matrix.

In all of the CASSCF calculations, a level shift of 5 au was used in order to improve convergence. In the CASPT2 calculations, none of the orbitals were frozen, and an imaginary level shift of 0.2 au was used to eliminate intruder states.²⁷

RESULTS AND DISCUSSION

IRPD spectroscopy: A representative IRPD spectrum of $[(\text{TMC})\text{Fe}(\text{O})(\text{CH}_3\text{CN})]^{2+}$ ion (**1**, TMC = 1,4,8,11-tetramethyl-1,4,8,11-tetraazacyclotetradecane) is shown in Figure 1. The $\text{Fe}=\text{O}$ vibration is at 848 cm^{-1} and shifts to 812 cm^{-1} upon ^{18}O labeling (Figure 1b). The theoretical IR spectrum calculated with the B3LYP/6-311+G* method (Figure 1c) provides an excellent prediction of the vibrational finger-print of the ligand, but the $\text{Fe}=\text{O}$ stretching frequency is shifted by 66 cm^{-1} to higher wavenumbers. Very similar results were obtained also for the rest of the complexes in Chart 1 (the spectra and the experimental conditions for all measurements can be found in the Supporting Information, Figures S4-S11, S13-S14).

The determined $\text{Fe}=\text{O}$ stretching vibrations are unique characteristics of the depicted ionic complexes. The values obtained by rR spectroscopy in solution (in italics in Chart 1) are determined with variable red shifts. It reflects the effect of the solvent as well as the effect of the counter ion. For the studied dications **1**, **4** $[(\text{N4Py})\text{Fe}(\text{O})]^{2+}$, N4Py = *N,N*-bis(2-pyridylmethyl)bis(2-pyridyl)methylamine) and **6** $[(\text{PyTACN})\text{Fe}(\text{O})(\text{CH}_3\text{CN})]^{2+}$, PyTACN = (1-[2'-(pyridyl)methyl]-4,7-dimethyl-1,4,7-triazacyclononane)), the solution spectral shifts of -9 cm^{-1} (for **1**) and -12 cm^{-1} (for **4** and **6**) with respect to the gas phase are observed. Interestingly, singly charged complex **3** is affected even more (-18 cm^{-1}).

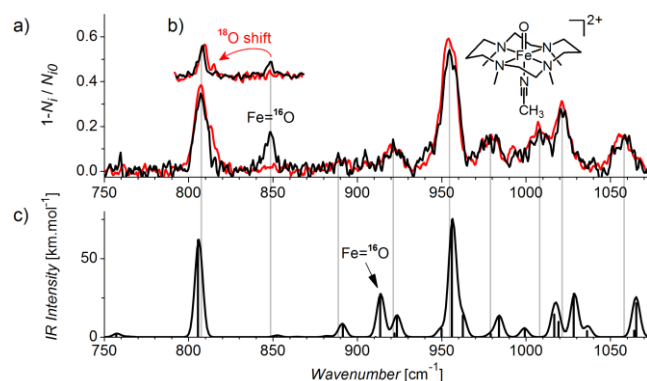


Figure 1. (a) Helium tagging IRPD spectrum of the $[(\text{TMC})\text{Fe}(\text{O})(\text{CH}_3\text{CN})]^{2+}$ (**1**); (b) the spectral range with $\text{Fe}=\text{O}$ and $\text{Fe}=\text{O}$ stretching vibrations measured with a higher resolution; (c) B3LYP/6-311+G* theoretical IR spectrum of $[(\text{TMC})\text{Fe}(\text{O})(\text{CH}_3\text{CN})]^{2+}$ (scaling factor is 0.99).

The big advantage of our method is that we can unequivocally characterize all species formed in solution by the speciation of the parent compound one by one (we transfer them to the gas-phase and study them after mass-selection). Hence, oxidation of $[(\text{PyTACN})\text{Fe}(\text{OTf})_2]$ in acetonitrile yields not only the $[(\text{PyTACN})\text{Fe}(\text{O})(\text{CH}_3\text{CN})]^{2+}$ dication (**6**), but also singly charged $[(\text{PyTACN})\text{Fe}(\text{O})(\text{OTf})]^+$ (**7**) bearing the triflate ion as a ligand. We have also characterized complexes with nitrate, trifluoroacetate, and perchlorate (**8**, **9**, and **10**). Gaseous dication **6** has the $\text{Fe}=\text{O}$ stretching vibration at 843 cm^{-1} . Coordination of nitrate and triflate (i.e. formation of **8** and **9**) induces a blue shift of the $\text{Fe}=\text{O}$ stretch by 7 cm^{-1} with respect

to **6**, whereas the other anions bring about a minor red-shift (Chart 1, Figures S10-S11, S13-S14).

We have correlated the available $\text{Fe}=\text{O}$ stretching vibrations determined in solution with the values determined in the gas-phase for all species theoretically present in solution (mono- as well as dications). The gas-phase values are in average 9 cm^{-1} blue-shifted (Figure 2). The shift is slightly larger (11 cm^{-1}), if we assume that the solutions contain only dications. Coordination of triflate to the iron center results in a redshift of the $\text{Fe}=\text{O}$ stretching vibration (*cf.* **6** vs. **7** and **1** vs. **2** in Figure 2). Interestingly, the $\text{Fe}=\text{O}$ stretch is significantly red-shifted even in complex **5** (with respect to **4**) that bears triflate as a non-coordinated counter ion as evidenced from its IRPD spectrum (Figure S8). The IRPD spectrum of **5** contains $\text{S}=\text{O}$ stretching bands that clearly correspond to a non-coordinated triflate ion. On contrary, **2** and **7** bear triflates as ligands. This is again evidenced by the triflate bands in the IRPD spectra of the complexes (Figures S5 and S13 in the SI).

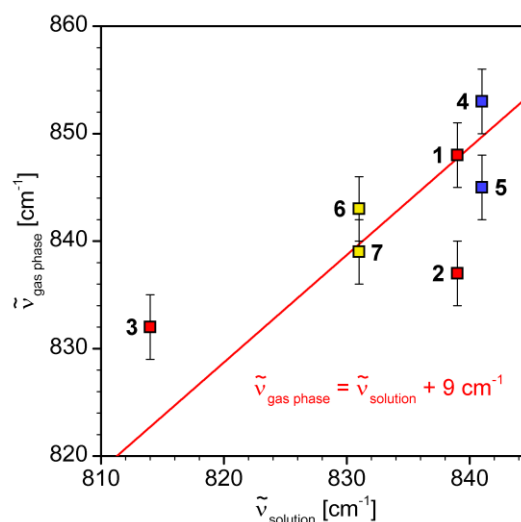


Figure 2. Comparison of the spectral shift of the $\text{Fe}=\text{O}$ stretching vibration of the studied complexes measured in the gas phase and in acetonitrile solution (complexes with the same ligand are color-coded: TMC – red, N4Py – blue, PyTACN – yellow).

The $[(\text{PyTACN})\text{Fe}(\text{O})(\text{X})]^+$ ($\text{X} = \text{OTf}, \text{CF}_3\text{COO}, \text{NO}_3, \text{ClO}_4$) complexes can exist in two isomeric forms - with the oxo group either in the equatorial or in the axial position (parallel or perpendicular to the pyridine ring plane). In addition, the complexes can be formed in the triplet ($S=1$) or in the quintet ($S=2$) state. According to the CASPT2 (Table 1), the $S=1$ isomer with the oxo in the equatorial position is favored in **8**, **9** and **10**. For the complex with the triflate ligand, both spin states are almost isoenergetic, with the high spin-state isomer $^57_{\text{eq}}$ being slightly preferred over $^37_{\text{eq}}$. The CASPT2 energies agree relatively well with the predictions obtained by the DFT using the B3LYP functional for **8** and **9**, but not for **7** and **10** (Table 1). We have tested several other DFT functionals. Most of them render relative energies of the spin-isomers completely wrong.²⁸ The B3LYP functional also outperforms the other functionals in the predictions of IR spectra.²⁹ A notable

exception is that pure DFT functionals, e.g. M06L, give a better estimate of the Fe=O frequency (but a worse description of the ligand skeletal vibrations; see Figures S15-S16).

To further substantiate the power of our approach, we have attempted to prepare axial isomers of $[(\text{PyTACN})\text{Fe}(\text{O})(\text{X})]^+$ by the gas phase elimination of the NO_2^\bullet radical from the $[(\text{PyTACN})\text{Fe}(\text{NO}_3)(\text{X})]^+$ precursors.³⁰ We have recently showed that this “nitrate cleavage method” for $[(\text{PyTACN})\text{Fe}(\text{NO}_3)_2]^+$ leads dominantly to the generation of the quintet state of the $[(\text{PyTACN})\text{Fe}(\text{O})(\text{NO}_3)]^+$ isomer with the oxo in the axial position ($^5\mathbf{8}_{\text{ax}}$).²⁸ Hence, next to the S=1 isomer $^3\mathbf{8}_{\text{eq}}$ obtained classically from solution, we have an independent access to the S=2 isomer $^5\mathbf{8}_{\text{ax}}$. We set to determine the difference in the Fe=O vibration frequency between these spin-isomers.

Comparison of the IRPD spectrum of $^3\mathbf{8}_{\text{eq}}$ and its ^{18}O labeled analog led to a clear assignment of the Fe=O band at 850 cm^{-1} (cf. Figure S10). Figure 3a shows the comparison of the spectra in the lower wavenumber range obtained for $^3\mathbf{8}_{\text{eq}}$ and $^5\mathbf{8}_{\text{ax}}$. The spectra were obtained as a difference between the spectra of ions generated from solution and by the nitrate cleavage (see Figure S10 in the Supporting Information).

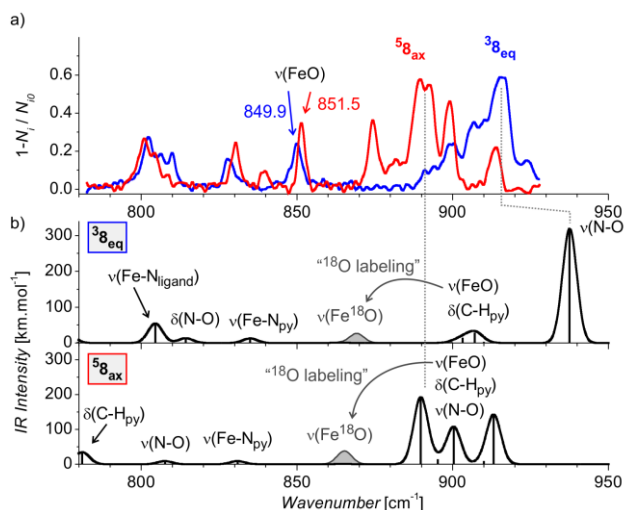


Figure 3. (a) IRPD difference spectra (cf. Figure S10) of the $[(\text{PyTACN})\text{Fe}(\text{O})(\text{NO}_3)]^+$ isomers generated by ligand exchange from the solution of $[(\text{PyTACN})\text{Fe}(\text{O})(\text{CH}_3\text{CN})]^{2+}$ (blue trace) and generated in the gas phase from $[(\text{PyTACN})\text{Fe}(\text{NO}_3)_2]^+$ by the nitrate cleavage (red trace). (b) Theoretically predicted spectra of $^3\mathbf{8}_{\text{eq}}$ and $^5\mathbf{8}_{\text{ax}}$ at the B3LYP-D3/6-311++G** level of theory scaled by 0.99. The predictions of the redshift of the Fe=O vibration upon ^{18}O labeling is shown in gray.

At the first sight, there is a large difference in the N-O stretching band position (as observed previously).²⁸ The position of the Fe=O stretching band is however almost identical. The Fe=O stretch of $^5\mathbf{8}_{\text{ax}}$ lies at 851.5 cm^{-1} . The difference is thus just 1 cm^{-1} . The agreement with the theoretical IR spectra is not great, but we show it in order to demonstrate that the large difference between the N-O stretches is expected, as well as the minor difference between the Fe=O stretches (as usually blue-shifted by almost 40 cm^{-1} in the theoretical spectra).

The nitrate cleavage approach to preparation of $[(\text{PyTACN})\text{Fe}(\text{O})(\text{CF}_3\text{COO})]^+$ provides – similarly as above – ions with the IRPD spectrum distinctly different from that of the analogous ions generated from solution (cf. the red and the black spectrum in Figure 4a).

Table 1. CASPT2 relative energies^b of different spin-isomers of $[(\text{PyTACN})\text{Fe}(\text{O})(\text{X})]^+$ complexes.

$E_{\text{tot,rel}}^{\text{a}} [\text{kcal mol}^{-1}], (E_{\text{rel}}^{\text{OK}} [\text{kcal mol}^{-1}])$				
Notation ^b	X	Spin	Energy CASPT2 ^a	Energy B3LYP
$^3\mathbf{7}_{\text{eq}}$	CF_3SO_3	S=1	0.0 (1.1)	0.0 (0.0)
$^3\mathbf{7}_{\text{ax}}$	CF_3SO_3	S=1	2.3 (3.6)	3.3 (3.1)
$^5\mathbf{7}_{\text{eq}}$	CF_3SO_3	S=2	0.1 (0.0)	2.0 (3.2)
$^5\mathbf{7}_{\text{ax}}$	CF_3SO_3	S=2	1.5 (1.4)	3.0 (4.3)
$^3\mathbf{8}_{\text{eq}}$	NO_3	S=1	0.0 (0.0)	0.0 (0.0)
$^3\mathbf{8}_{\text{ax}}$	NO_3	S=1	2.6 (2.4)	2.6 (2.8)
$^5\mathbf{8}_{\text{eq}}$	NO_3	S=2	2.1 (1.5)	3.0 (3.6)
$^5\mathbf{8}_{\text{ax}}$	NO_3	S=2	0.4 (0.0)	0.7 (1.1)
$^3\mathbf{9}_{\text{eq}}$	CF_3COO	S=1	0.0 (0.0)	0.0 (0.0)
$^3\mathbf{9}_{\text{ax}}$	CF_3COO	S=1	5.2 (5.0)	4.7 (4.5)
$^5\mathbf{9}_{\text{eq}}$	CF_3COO	S=2	3.0 (2.5)	3.9 (3.4)
$^5\mathbf{9}_{\text{ax}}$	CF_3COO	S=2	3.5 (2.8)	4.0 (3.3)
$^3\mathbf{10}_{\text{eq}}$	ClO_4	S=1	1.0 (2.6)	0.0 (0.0)
$^3\mathbf{10}_{\text{ax}}$	ClO_4	S=1	3.2 (4.9)	3.3 (3.2)
$^5\mathbf{10}_{\text{eq}}$	ClO_4	S=2	0.0 (0.0)	1.6 (3.2)
$^5\mathbf{10}_{\text{ax}}$	ClO_4	S=2	3.7 (4.7)	2.1 (2.7)

a) Calculations were performed by CASPT2(12,9)/ANO-RCC at geometries optimized at B3LYP-D3 level of theory as described in the experimental details. The numbers in brackets are the CASPT2 energies corrected by zero-point vibrational energy calculated at the B3LYP-D3 level.

b) The index refers to the $[(\text{PyTACN})\text{Fe}(\text{O})(\text{X})]^+$ isomer with the oxo group in the equatorial (eq) or axial (ax) position

Detailed inspection shows that the spectrum of ions transferred from the solution of iron(IV) complex is composed of two components (upper trace). In addition to the bands present in the spectrum of the gas-phase generated ions (middle trace), there are also several unique bands. We have subtracted the spectrum of the gas-phase generated ions and obtained the IR spectrum of the second component (lower trace; for the details of the spectra separation see the SI, Figure S12). The major difference is located in the range $1130 - 1180\text{ cm}^{-1}$. The B3LYP analysis shows that the observed bands correspond to the C-F vibrations. These vibrations are influenced by the spin state of the complex. In theory, the lowest-energy C-F vibrational band of the S=1 complexes is red shifted with respect to the corresponding band of the S=2 complexes. Opposite, but less pronounced shift can be observed for the C=O vibration and the other C-F vibrations (cf. Figure 4b). Analogous differences stand out if we compare the red and blue spectrum in Figure 4a.

As a result, we assign the red spectrum (ions generated by the nitrate cleavage) to the S=2 complexes (the lowest lying

C-F vibration band is blue shifted, whereas the C=O vibration is red-shifted with respect to the bands in the blue spectrum). The blue spectrum accordingly corresponds to the $S=1$ complexes. Electrospray ionization of the complexes oxidized in solution thus leads to a mixture of the spin-isomers (black spectrum).

The separation process provides an estimate that about 30% of the complexes transferred from the solution should be in the quintet state (see Figure S12). The probable reasoning is that the solution dominantly contains dication $^3\mathbf{6}$ that coordinates CF_3COO^- during the electrospray process. If trifluoroacetate coordinates to the equatorial position, it leads to $^5\mathbf{9}_{\text{ax}}$ – the more stable spin-isomer with the oxo in the axial position. Alternatively, the coordination of the anion to the axial position leads to the formation of $^3\mathbf{9}_{\text{eq}}$. This line of reasoning also explains why nitrate coordinated complexes $\mathbf{8}$ are obtained from the oxidized solution in a similar ratio of $^3\mathbf{8}_{\text{eq}}$ to $^5\mathbf{8}_{\text{ax}}$ (see separation in Figure S10).²⁸

Preparations of different spin-isomers with the triflate and perchlorate ligands ($[(\text{PyTACN})\text{Fe}(\text{O})(\text{OTf})]^+$ ($\mathbf{7}$) and $[(\text{PyTACN})\text{Fe}(\text{O})(\text{ClO}_4)]^+$ ($\mathbf{10}$)) were not successful. The IRPD spectra of the complexes with the perchlorate ligand were identical regardless of their preparation (*i.e.* transfer from solution or by nitrate cleavage). For the $[(\text{PyTACN})\text{Fe}(\text{O})(\text{OTf})]^+$ complexes, the IRPD spectrum of the ions prepared in the gas phase by the “nitrate cleavage” differs from that of the ions generated from solution, but the differences are not due to the expected change of the spin-isomer. The detected additional bands rather suggest presence of isobaric ions with an oxidized ligand. Most probably, the initially generated quintet state isomers formed upon the nitrate cleavage are very reactive and the iron(IV)-oxo moiety attacks the ligand (probably at one of the nitrogen atoms of the ligand, forming the corresponding amine *N*-oxide, *cf.* Figure S13).³¹ The prediction of the theoretical spectra is not sufficiently accurate to allow us to unequivocally assign the spin states of $\mathbf{7}$ and $\mathbf{10}$ (Figures S6, S7). Without an access to both spin-states, we cannot judge the band shifts in the spectrum.

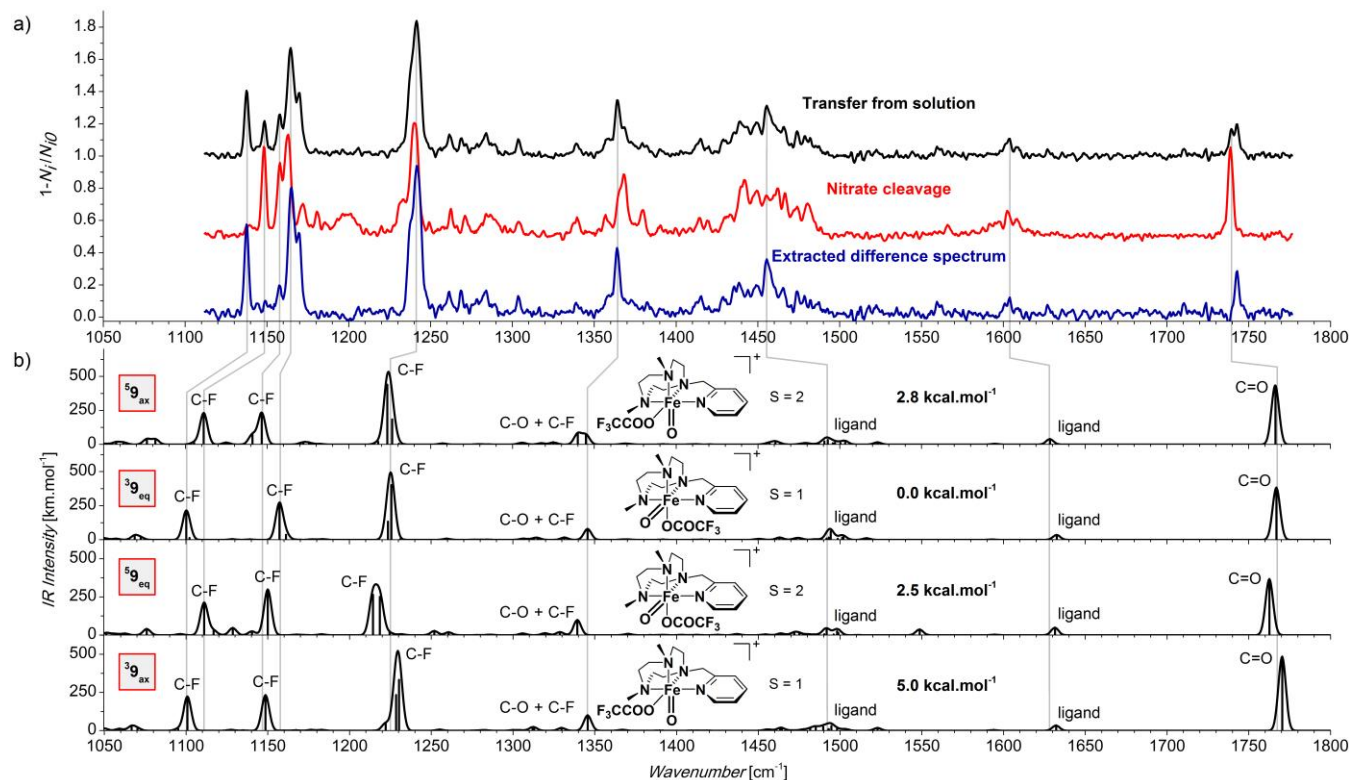


Figure 4. (a) IRPD spectra of the $[(\text{PyTACN})\text{Fe}(\text{O})(\text{CF}_3\text{COO})]^+$ isomers generated by ligand exchange from the solution of $[(\text{PyTACN})\text{Fe}(\text{O})(\text{CH}_3\text{CN})]^{2+}$ (the upper trace), generated in the gas phase from $[(\text{PyTACN})\text{Fe}(\text{NO}_3)(\text{CF}_3\text{COO})]^+$ by the nitrate cleavage (the middle trace) and the extracted difference spectrum (the lowest trace). (b) Theoretically predicted spectra of various isomers at the B3LYP-D3/BS1 level of theory scaled by 0.99. Energies are calculated at the CASPT2 level (see Table S1 for absolute values) with DFT zero-point energy corrections.

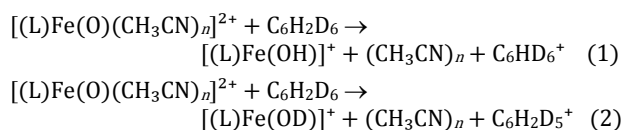
Table 2. Reactivities of [(L)Fe(O)(X)]^{2+/+} complexes with 1,4-cyclohexadiene-1,2,3,4,5,6-d₆ in the gas phase.^a

Entry	L/X	from ^a	Total reactivity ^b	Branching [%] HAT:DAT:OAT	KIE
1	TMC/CH ₃ CN (1)	sol.	360 ± 190	72:28: 0 ^c	2.5 ± 0.6
2	TMC/CF ₃ SO ₃ (2)	sol.	<3	-	-
3	N4Py/- (4)	sol.	10 ± 6	85:15: 0 ^{c,d}	5.7 ± 2.1
4	N4Py/CF ₃ SO ₃ (5)	sol.	5 ± 2	56:15:29	3.7 ± 0.4; (6.8) ^e
5	PyTACN/CH ₃ CN (6)	sol.	900 ± 400	79:21: 0 ^c	3.8 ± 0.5
6	PyTACN/CF ₃ SO ₃ (7)	sol.	454 ± 11	56:16:28	3.5 ± 0.3
7	PyTACN/CF ₃ SO ₃ (7)	frag.	187 ± 46 ^f	56:13:31	4.3 ± 0.2
8	PyTACN/NO ₃ (8)	sol.	100 ± 8	78:14: 8	5.6 ± 0.1
9	PyTACN/NO ₃ (8)	frag.	195 ± 10	74:16:10	4.6 ± 0.3
10	PyTACN/CF ₃ COO (9)	sol.	67 ± 13	76:14: 9	5.4 ± 1.4
11	PyTACN/CF ₃ COO (9)	frag.	238 ± 52	72:16:12	4.5 ± 0.2
12	PyTACN/ClO ₄ (10)	sol.	260	63:17:20	3.7
13	PyTACN/ClO ₄ (10)	frag.	261 ± 12	59:16:25	3.7 ± 0.3

- a) The [(PyTACN)Fe(O)(X)]⁺ complexes were generated by oxidation in solution and transferred by ESI to the gas phase (denoted as sol.) or by a fragmentation of their iron(III) nitrate precursors during the electrospray process (denoted as frag.)
- b) Total reactivity (sum of the rate constants for HAT, DAT, and OAT) is given relative to the reactivity of [(PyTACN)Fe(O)(NO₃)]⁺ transferred from the solution, which was determined to be $(8.4 \pm 3.1) \times 10^{-12} \text{ cm}^3 \cdot \text{s}^{-1}$ (Ref. 31) and is set as 100 here.
- c) For dications, we observe a transfer of H⁺/D⁺ instead of HAT and DAT (reactions 1 and 2 in the text). Note that for **1** and **6** the H⁺/D⁺ transfer is associated with elimination of acetonitrile
- d) We have observed also the electron transfer channel (7 % with respect to the total reactivity). We assume that this channel is due to a reaction with an impurity. See the Supporting Information for details.
- e) The measured KIE is affected by a presence of an isobaric impurity (*m/z* 588) which undergoes a Coulomb explosion to ions with *m/z* 586 and *m/z* 589. After subtraction of this impurity we obtain a KIE of 6.8.
- f) Note that this number is hampered by the fact that we worked with a mixture of **7** with unreactive Fe^{II} complexes with oxidized ligand.

Reactivity of the complexes: The access to the characterized iron(IV)-oxo complexes provides an opportunity to compare their unique reactivities. We have used 1,4-cyclohexadiene-1,2,3,4,5,6-d₆ as a probe reactant, because it enables us to compare hydrogen-atom transfer (HAT), deuterium-atom transfer (DAT), and oxygen-atom transfer (OAT) in one step (Table 1, Figures S18-S23).

Firstly, we have compared doubly charged iron(IV)-oxo complexes with different ligands (**1**, **4** and **6**). Gaseous reactions of dications with neutral molecules lead usually to the formation of two singly charged ions.³² Here, we observe H⁺ and D⁺ transfers instead of HAT and DAT. Formation of two singly charged ions from a dication-neutral couple is usually rather exothermic. Gaseous ions cannot dissipate the energy excess to solvent molecules. Instead, they undergo subsequent fragmentations. Here, we see a subsequent elimination of the acetonitrile molecule from complexes **1** and **6** (reactions 1 and 2; *n* = 1 for **1** and **6** and *n* = 0 for **4**). We do not see the OAT channel in the reactivity of dications. We note that the observed reactivity that suppresses formation of doubly charged products can be a sole property of gaseous complexes, because of the lack of solvation that would stabilize the doubly charged products. Nevertheless, there might be some relevance to condensed phase reactions (see refs. 33-35).



The total reactivities of the dicationic complexes can be ordered as **6** > **1** >> **4** (Entries 5, 1, and 3 in Table 2). This result is not in agreement with previously observed reactivities of these ions in solution with weak C-H bonds, such as in 9,10-dihydroanthracene, that can be ordered according to ligands as PyTACN ≈ N4Py > TMC (Figure S18 in the SI). The differences can arise from a solvent effect or from the involvement of the present anions.

All complexes were generated from their triflate precursors, we have therefore compared the reactivities of the respective monocations **2**, **5**, and **7** bearing triflate as a ligand (Entries 2, 4 and 6 in Table 2). The singly charged complexes follow the expected reaction channels: hydrogen-atom transfer, deuterium-atom transfer, and oxygen-atom transfer. Oxygen-atom transfer shows no KIE indicating that the reaction corresponds to the epoxidation of the double bond (cf. Table S2 in the Supporting Information). Somewhat surprisingly, the

total reactivities of monocations **5** (N4Py ligand) and **7** (PyTACN ligand) are on the same order of magnitude as those of the respective dications. On the other hand, the singly charged complex with the TMC ligand, **2**, is unreactive under the same conditions. This probably stems from the nature of coordination of the anionic ligand. Triflate is *cis*-coordinated to the oxo group in complex **7**, which leads to about 50% drop in the total reactivity (*cf.* Entry 5 and 6 in Table 2). Complex **5** contains triflate as loosely bound counter ions (the IRPD spectrum of complex **5** shows that triflate is not coordinated to iron, see Figure S8 in the SI). This loose binding leads also to about 50% reactivity drop (*cf.* Entry 3 and 4 in Table 2). Finally, the TMC ligand allows coordination of triflate only in the *trans*-position with respect to the oxo group, which is probably the reason of the drastic attenuation of the observed total reactivity.

The formation of the triflate-coordinated complexes **2** can thus affect the overall reactivity of the TMC complexes by decreasing a number of the reactive species **1** in solution. The same process should not significantly influence the reactivity of the complexes with N4Py and PyTACN ligands. It can thus explain the observed reactivity trend in the condensed phase (Figure S18 in the SI).

We have further compared relative reactivities in dependence of the anionic ligand and the spin state for complexes **7** – **10** (Entries 6 – 13 in Table 2). The reactivities decrease in the following order: **7** > **10** > $^5\mathbf{9}_{ax}$ > $^5\mathbf{8}_{ax}$ > $^3\mathbf{8}_{eq}$ > $^3\mathbf{9}_{eq}$ (we did not assign the spin-isomers of **7** and **10**, see above). The S=2 spin-isomers of **8** and **9** are more reactive than their S=1 analogs. With the increasing reactivity the kinetic isotope effect for HAT vs. DAT clearly decreases. Further, the relative abundance of the OAT channel correlates with the total reactivity. Its ratio increases with the increasing total reactivity. This channel is much more sensitive to the nature of the anion ligand than to the spin-state of the complex (*cf.* Figure 4).

We have also measured reactivities of the gas-phase generated **7** and **10**. As mentioned above, for complex **10** this method leads to the ions with identical spectral characteristics as the ions transferred from the oxidized solution. In agreement, the reactivities of the ions generated in both ways are identical. We can easily rationalize this result based on the quantum chemical calculations. The perchlorate ligand preferentially occupies the axial position of the complex in both spin-states (*i.e.* the oxo group is always in the equatorial position - $^3\mathbf{10}_{eq}$ and $^5\mathbf{10}_{eq}$ are the preferred spin-isomers). The CASPT2 calculations predict that the quintet state isomer $^5\mathbf{10}_{eq}$ is preferred in the gas-phase. Regardless, whether we transfer or generate S=1 or S=2 state during the electrospray ionization, we expect that due to the fast spin-isomerization at the iron center, we always detect reactivity of the preferred spin-isomer (*i.e.* $^5\mathbf{10}_{eq}$).

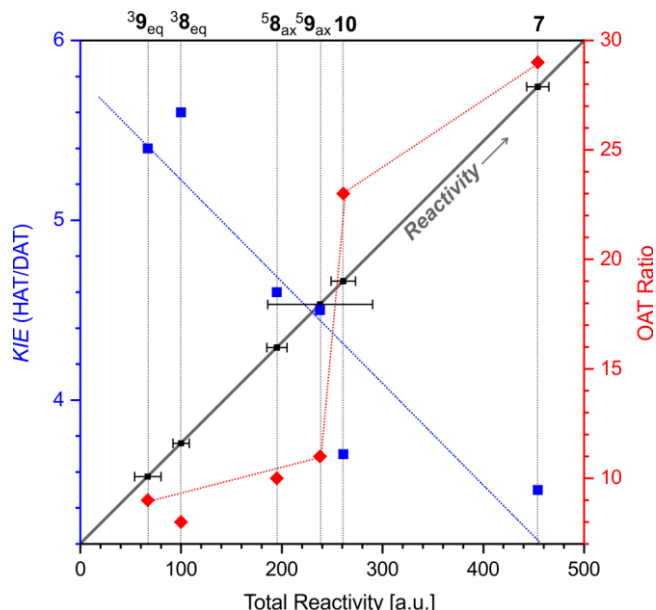


Figure 4. Comparison of gas-phase reactivity of complexes **7** – **10** with 1,4-cyclohexadiene-1,2,3,4,5,6- d_6 (see also Table 2). The error bars denote the standard deviation of the total reactivities. The dotted lines serve as a guide for eyes.

For the triflate-bound complex **7**, the reactivity of the ions generated by the gas-phase fragmentation significantly drops. This is also in accordance with our spectroscopic experiments that showed that these ions are contaminated by the isomers with oxidized ligand. Triflate, similarly to perchlorate, always occupies the axial position. We have therefore the same situation as for **10**. We generate a mixture of $^3\mathbf{7}_{eq}$ and $^5\mathbf{7}_{eq}$ that rapidly spin-isomerizes to the preferred spin-state in the gas phase (the CASPT2 calculations predict both of the spin-isomers to be essentially isoenergetic). We rationalize the drop in reactivity for the complexes generated by the nitrate cleavage by the large reactivity of the triflate complexes (*cf.* Table 2). The gas-phase generated ions are initially formed with a large internal energy excess. Under the same conditions, we are able to thermalize the less reactive ions (**8**, **9**, and **10**) by collisional cooling with the sheaths gas (N_2) before they undergo the internal oxidation. For complex **7**, the internal oxidation proceeds probably much faster and therefore a substantial amount of ions isomerizes before we are able to cool them to a low temperature.

CONCLUSIONS

We present helium tagging infrared spectroscopy as a unique tool to characterize iron(IV)-oxo complexes. We can unequivocally determine the Fe=O vibration as well as other spectral features in mass-selected reactive complexes. We have shown the comparison of gas-phase features with known data from solution. We show that solvation influences the Fe=O vibration. In acetonitrile, an average red-shift of 9 cm^{-1} was observed. Further, we have compared reactivities of the characterized gaseous complexes towards 1,4-cyclohexadiene. We show that the anions coordinated as ligands have a substantial effect on the reactivities and it depends on the nature of the anion as well as on the ligand. Comparison of relative

reactivities suggests that it might be necessary to include the counter-ion effect when comparing the reactivities of the complexes in solution. We further show that the anionic ligands influence the relative stabilities of the S=1 and S=2 states and play a role in oxygen-transfer reactions towards C-H bonds. For complex **8** that we were able to generate as two spin isomers ($^3\mathbf{8}_{\text{eq}}$ and $^5\mathbf{8}_{\text{ax}}$), we established that the Fe=O vibration differs only by 1 cm⁻¹. We demonstrate that the S=1 and S=2 states can be distinguished based on the vibrations of the anionic ligands.

ASSOCIATED CONTENT

Supporting Information

Further experimental details, all experimental and calculated spectra, gas-phase reactivities, theoretical results, calculated structures (in XYZ format) and complete reference 18. This material is available free of charge via the Internet at <http://pubs.acs.org>.

AUTHOR INFORMATION

Corresponding Authors

* roithova@natur.cuni.cz

* miquel.costas@udg.edu

* martin.srnec@jh-inst.cas.cz

Notes

The authors declare no competing financial interests.

ACKNOWLEDGMENT

Computational resources were provided by the MetaCentrum under the program LM2010005 and the CERIT-SC under the program Centre CERIT Scientific Cloud, part of the Operational Program Research and Development for Innovations, Reg. no. CZ.1.05/3.2.00/08.0144. The project was supported by the Czech Science Foundation (14-20077S and 15-10279Y), European Research Council (ERC CoG No. 682275), and the COST action ECOSTBio. MS is also grateful to the Czech Academy of Sciences for the Purkyně fellowship.

REFERENCES

- (1) (a) Abu-Omar, M. M.; Loaiza, A.; Hontzeas, N. *Chem. Rev.* **2005**, *105*, 2227–2252. (b) Stone, K. L.; Borovik, A. S. *Curr. Opin. Chem. Biol.* **2009**, *13*, 114–118. (c) Solomon, E. I.; Light, K. M.; Liu, L. V.; Srnc, M.; Wong, S. D. *Acc. Chem. Res.* **2013**, *46*, 2725–2739. (d) Cho, K.-B.; Hirao, H.; Shaik, S.; Nam, W. *Chem. Soc. Rev.* **2016**, *45*, 1197. (e) Usharani, D.; Janardanan, D.; Li, C.; Shaik, S. *Acc. Chem. Res.* **2013**, *46*, 471–482. (2) (a) Price, J. C.; Barr, E. W.; Tirupati, B.; Bollinger, J. M., Jr.; Krebs, C. *Biochemistry* **2003**, *42*, 7497. (b) Bollinger, J. M., Jr.; Krebs, C. *J. Inorg. Biochem.* **2006**, *100*, 586. (c) Krebs, C.; Galonić Fujimori, D.; Walsh, C. T.; Bollinger, J. M., Jr. *Acc. Chem. Res.* **2007**, *40*, 484. (3) (a) Nam, W. *Acc. Chem. Res.* **2007**, *40*, 522–531. (b) Nam, W.; Lee, Y.-M.; Fukuzumi, S. *Acc. Chem. Res.* **2014**, *47*, 1146–1154. (c) Ray, K.; Pfaff, F. F.; Wang, B.; Nam, W. *J. Am. Chem. Soc.* **2014**, *136*, 13942–13958. (4) (a) McDonald, A. R.; Que, L., Jr. *Coord. Chem. Rev.* **2013**, *257*, 414–428. (b) Puri M.; Que, L.; Jr. *Acc. Chem. Res.* **2015**, *48*, 2443–2452. (5) J.-U. Rohde, J.-H. In, M.-H. Lim, W. W. Brennessel, M. R. Bukowski, A. Stubna, E. Münck, W. Nam, J. Que, L., *Science* **2003**, *299*, 1037–1039. (6) (a) Klein, J.E.M.N.; Que, L., Jr. Biomimetic High-Valent Mononuclear Nonheme Iron-Oxo Chemistry. In *Encyclopedia of Inorganic and Bioinorganic Chemistry*; R.A. Scott, Ed.; John Wiley: Chichester, 2016 (b) Hohenberger, J.; Ray, K.; Meyer, K. *Nat. Commun.* **2012**, *3*, 720. (7) Sastri, C. V.; Park, M. J.; Ohta, T.; Jackson, T. A.; Stubna, A.; Seo, M. S.; Lee, J.; Kim, J.; Kitagawa, T.; Munck, E.; Que, L., Jr.; Nam, W. *J. Am. Chem. Soc.* **2005**, *127*, 12494–12495. (8) (a) Rohde, J.-U.; Stubna, A.; Bominaar, E. L.; Munck, E.; Nam, W.; Que, L., Jr. *Inorg. Chem.* **2006**, *45*, 6435–6445. (b) Planas, O.; Clemancey, M.; Latour, J.-M.; Company, A.; Costas, M. *Chem. Commun.* **2014**, *50*, 10887–10890. (9) Ye, S.; Kupper, C.; Meyer, S.; Andris, E.; Navratil, R.; Krahe, O.; Mondal, B.; Atanasov, M.; Bill, E.; Roithova, J.; Meyer, F.; Neese, F. *J. Am. Chem. Soc.* **2016**, *138*, 14312–14325. (10) McLuckey, S. A.; Wells, J. M. *Chem. Rev.* **2001**, *101*, 571–606. (11) (a) To, W. P.; Chow, T. W.-S.; The, C.-W.; Guan, X.; Huang, J.-S.; Che, C.-M. *Chem. Sci.* **2015**, *6*, 5891. (b) Prat, I.; Mathieson, J. S.; Güell, M.; Ribas, X.; Luis, J. M.; Cronin, L.; Costas, M. *Nature Chem.* **2011**, *3*, 788. (c) Hitomi, Y.; Arakawa, K.; Funabiki, T.; Kodera, M. *Angew. Chem. Int. Ed.* **2012**, *51*, 3448–3452. (12) Theron, R.; Yang, W.; Yunker, L. P. E.; Hesketh, A. V.; Pernik, I.; Weller, A. S.; McIndoe, J. S. *ACS Catal.* **2016**, *6*, 6911–6917. (13) (a) Douberly, G. E.; Walters, R. S.; Cui, J.; Jordan, K. D.; Duncan, M. A. *J. Phys. Chem. A*, **2010**, *114*, 4570–4579. (b) Rizzo, T. R.; Boyarkin, O. V. *Top. Curr. Chem.* **2015**, *365*, 43–97. (c) Heine, N.; Fagiani, M. R.; Rossi, M.; Wende, T.; Berder, G.; Blum, V.; Asmis, K. R. *J. Am. Chem. Soc.*, **2013**, *135*, 8266–8273. (d) Wolk, A. B.; Leavitt, C. M.; Garand, E.; Johnson, M. A. *Acc. Chem. Res.* **2014**, *47*, 202–210. (14) (a) Roithová, J.; Gray, A.; Andris, E.; Jašík, J.; Gerlich, D. *Acc. Chem. Res.* **2016**, *49*, 223–230. (b) Jašík, J.; Gerlich, D.; Roithová, J. *J. Am. Chem. Soc.* **2014**, *136*, 2960 – 2962. (c) Jašík, J.; Navrátil, R.; Němec, I.; Roithová, J. *J. Phys. Chem. A* **2015**, *119*, 12648 – 12655. (d) Schulz, J.; Jašík, J.; Gray, A.; Roithová, J. *Chem. Eur. J.* **2016**, *22*, 9827 – 9834. (15) (a) Seo, M. S.; In, J.-H.; Kim, S. O.; Oh, N. Y.; Hong, J.; Kim, J.; Que, L., Jr.; Nam, W. *Angew. Chem. Int. Ed.* **2004**, *43*, 2417–2420. (b) Puri, M.; Company, A.; Sabenya, G.; Costas, M.; Que, L., Jr. *Inorg. Chem.* **2016**, *55*, 5818–5827. (16) (a) Ducháčková, L.; Roithová, J. *Chem. Eur. J.* **2009**, *15*, 13399. (b) Jašíková, L.; Roithová, J. *Organometallics* **2012**, *31*, 1935. (17) (a) Company, A.; Prat, I.; Frisch, J. R.; Ballesté, R. M.; Güell, M.; Juhász, G.; Ribas, X.; Münck, E.; Luis, J. M.; Que, L., Jr.; Costas, M. *Chem. Eur. J.* **2011**, *17*, 1622–1634. (b) Sastri, C. V.; Lee, J.; Oh, K.; Lee, Y. J.; Lee, J.; Jackson, T. A.; Ray, K.; Hirao, H.; Shin, W.; Halfen, J. A.; Kim, J.; Que, L.; Shaik, S.; Nam, W. *Proc. Natl. Acad. Sci.* **2007**, *104*, 19181–19186. (18) Ervin, K. M.; Armentrout, P. B. *J. Chem. Phys.* **1985**, *83*, 166–189. (19) Jašík, J.; Žabka, J.; Roithová, J.; Gerlich, D. *Int. J. Mass Spectrom.* **2013**, *354–355*, 204–210. (20) Gaussian 09, Revision D.01, Frisch, M. J. et al. Gaussian, Inc., Wallingford CT, 2013. (21) (a) Jensen, F. *J. Chem. Phys.* **2001**, *115*, 9113. (b) Jensen, F. *J. Chem. Phys.* **2002**, *116*, 7372. (c) Jensen, F.; Helgaker, T.; *J. Chem. Phys.* **2004**, *121*, 3463. (22) Boese, A. D.; Martin, J. M. L. *J. Mol. Struct.* **2006**, *780–781*, 310–316. (23) (a) Roos, B. O.; Taylor, P. R.; Siegbahn, P. E. M. *Chem. Phys.* **1980**, *48*, 157–173. (b) Siegbahn, P. E. M.; Almlöf, J.; Heiberg, A.; Roos, B. O. *J. Chem. Phys.* **1981**, *74*, 2384–2396. (24) (a) Andersson, K.; Malmqvist, P.-Å.; Roos, B. O.; Sadlej, A. J.; Wolinski, K.; *J. Phys. Chem.* **1990**, *94*, 5483–5488. (b) Andersson, K.; Malmqvist, P.-Å.; Roos, B. O. *J. Chem. Phys.* **1992**, *96*, 1218–1226. (c) Andersson, K. *Theor. Chim. Acta* **1995**, *91*, 31–46. (d) Finley, J.;

- Malmqvist, P.-Å.; Roos, B. O.; Serrano-Andrés, L. *Chem. Phys. Lett.* **1998**, *288*, 299-306.
- (25) Aquilante, F.; Pedersen, T. B.; Lindh, R.; Roos, B. O.; Sánchez de Merás, A.; Koch, H. J. *Chem. Phys.* **2008**, *129*, 024113.
- (26) (a) Douglas, M.; Kroll, N. M.; Ann. Phys. (N.Y.) **1974**, *82*, 89-155. (b) Hess, B. A.; Phys. Rev. A **1986**, *33*, 3742-3748. (c) Jansen, G.; Hess, B. A. *Phys. Rev. A* **1989**, *39*, 6016-6017.
- (27) (a) Roos, B. O.; Andersson, K.; *Chem. Phys. Lett.* **1995**, *245*, 215-243. (b) Forsberg, N.; Malmqvist, P.-Å. *Chem. Phys. Lett.* **1997**, *274*, 196-204.
- (28) Andris, E.; Jašík, J.; Gómez, L.; Costas, M.; Roithová, J. *Angew. Chem. Int. Ed.* **2016**, *55*, 3637-3641.
- (29) (a) Duffy, E. M.; Marsh, B. M.; Voss, J. M.; Garand, E. *Angew. Chem. Int. Ed.* **2016**, *55*, 4079-4082. (b) Škríba, A.; Jašík, J.; Andris, E.; Roithová, J.; *Organometallics* **2016**, *35*, 990-994. (c) Fridgen, T. D. *Mass Spectrom. Rev.* **2009**, *28*, 586-607. (d) Nosenko, Y.; Menges, F.; Riehn, C.; Niedner-Schatteburg, G. *Phys. Chem. Chem. Phys.* **2013**, *15*, 8171-8178. (e) Ingram, J.; Wolk, A. B.; Flender, C.; Zhang, J.; Johnson, C. J.; Hintermair, U.; Crabtree, R. H.; Johnson, M. A.; Zare, R. N. *Inorg. Chem.* **2014**, *53*, 423-433. (f) Jašíková, L.; Hanikýřová, E.; Schröder, D.; Roithová, J. *J. Mass Spectrom.* **2012**, *47*, 460-465. (g) Jašíková, L.; Hanikýřová, E.; Škríba, A.; Jašík, J.; Roithová, J. *J. Org. Chem.* **2012**, *77*, 2829-2936. (h) Roithová, J.; Milko, P. *J. Am. Chem. Soc.* **2010**, *132*, 281-288. (i) Chiavarino, B.; Crestoni, M. E.; Fornarini, S.; Lanucara, F.; Lemaire, J.; Maitre, P. *Angew. Chem., Int. Ed.* **2007**, *46*, 1995-1998.
- (30) Schröder, D.; Roithová, J.; Schwarz, H. *Int. J. Mass Spectrom.* **2006**, *254*, 197-201.
- (31) Nielsen, A.; Larsen, F. B.; Bond, A. D.; McKenzie, C. J. *Angew. Chem. Int. Ed.* **2006**, *45*, 1602-1606.
- (32) Roithová, J.; Schröder, D. *Phys. Chem. Chem. Phys.* **2007**, *9*, 2341-2349.
- (33) Kim, S.; Cho, K.-B.; Lee, Y.-M.; Chen, J.; Fukuzumi, S.; Nam, W. *J. Am. Chem. Soc.* **2016**, *138*, 10654-10663.
- (34) Oloo, W. N.; Feng, Y.; Iyer, S.; Parmelee, S.; Xue, G.; Que, L., Jr. *New J. Chem.* **2013**, *37*, 3411-3415.
- (35) Kwon, Y. H.; Mai, B. K.; Lee, Y.-M.; Dhuri, S. N.; Mandal, D.; Cho, K.-B.; Kim, Y.; Shaik S.; Nam, W. J. *Phys. Chem. Lett.* **2015**, *6*, 1472-1476.

